Pilz, M., Parolai, S., Picozzi, M., Wang, R., Leyton, F., Campos, J., Zschau, J. (2010): Shear wave velocity model of the Santiago de Chile basin derived from ambient noise measurements: A comparison of proxies for seismic site conditions and amplification. - Geophysical Journal International, 182, 1, pp. 355—367.

DOI: http://doi.org/10.1111/j.1365-246X.2010.04613.x

Geophysical Journal International

Geophys. J. Int. (2010) **182,** 355–367 doi: 10.1111/j.1365-246X.2010.04613.x

Shear wave velocity model of the Santiago de Chile basin derived from ambient noise measurements: a comparison of proxies for seismic site conditions and amplification

Marco Pilz,[1,2] Stefano Parolai,[1] Matteo Picozzi,[1] Rongjiang Wang,[1] Felipe Leyton,[3] Jaime Campos[4] and Jochen Zschau[1]

[1] *Helmholtzzentrum Potsdam, German Research Center for Geosciences, Telegrafenberg,* 14473 *Potsdam, Germany. E-mail: pilz@gfz-potsdam.de*
[2] *Universität Potsdam, Institut für Geowissenschaften, Karl-Liebknecht-Str.* 24, 14476 *Potsdam, Germany*
[3] *Universidad de Talca, Dept. de Construccion Civil, Curicó, Chile*
[4] *Universidad de Chile, Dept. de Geofisica, Blanco Encalada* 2002, *Santiago, Chile*

Accepted 2010 April 1. Received 2010 January 18; in original form 2009 October 23

SUMMARY

We determined a high-resolution 3-D *S*-wave velocity model for a 26 km × 12 km area in the northern part of the basin of Santiago de Chile. To reach this goal, we used microtremor recordings at 125 sites for deriving the horizontal-to-vertical (H/V) spectral ratios that we inverted to retrieve local *S*-wave velocity profiles. In the inversion procedure, we used additional geological and geophysical constraints and values of the thickness of the sedimentary cover already determined by gravimetric measurements, which were found to vary substantially over short distances in the investigated area. The resulting model was derived by interpolation with a kriging technique between the single *S*-wave velocity profiles and shows locally good agreement with the few existing velocity profile data, but allows the entire area, as well as deeper parts of the basin, to be represented in greater detail. The wealth of available data allowed us to check if any correlation between the *S*-wave velocity in the uppermost 30 m (v_S^{30}) and the slope of topography, a new technique recently proposed by Wald and Allen, exists on a local scale. We observed that while one lithology might provide a greater scatter in the velocity values for the investigated area, almost no correlation between topographic gradient and calculated v_S^{30} exists, whereas a better link is found between v_S^{30} and the local geology. Finally, we compared the v_S^{30} distribution with the MSK intensities for the 1985 Valparaiso event, pointing out that high intensities are found where the expected v_S^{30} values are low and over a thick sedimentary cover. Although this evidence cannot be generalized for all possible earthquakes, it indicates the influence of site effects modifying the ground motion when earthquakes occur well outside of the Santiago basin.

Key words: Site effects; Sedimentary basin; South America.

1 INTRODUCTION

Extended mountain valleys with wide plains of fluvial deposits or lakeshores and estuaries with water-saturated sediments are particularly prone to seismic site amplification and nonlinear effects. In former times, such seismically unfavourable sites would have been attractive for spacious settlements and industries, and many cities worldwide have grown extensively over such plains and are still expanding. Given this spread of urban populations into areas of unfavourable soils, future earthquakes might cause extensive human and economic damage because geometrical and mechanical features of alluvial deposits have a great influence on seismic wave propagation and amplification. Therefore, knowledge of the mechanical characteristics of the underlying soil is of broad interest and may contribute to seismic hazard assessment.

In general, two main types of site effects can be distinguished: stratigraphic effects due to the velocity contrast between the sedimentary soil layers on the one hand (Bard & Bouchon 1985; Sánchez-Sesma & Luzon 1995; Bielak *et al.* 1999; Chávez-García *et al.* 1999) as well as topographic effects due to focusing and/or scattering effects around crests and hills (Bouchon 1973; Paolucci 2002; Semblat *et al.* 2002). Hence, the seismic response might be influenced both by the local geology, which often leaves significant imprint on seismic motion by amplifying the amplitudes of seismic waves and increasing the shaking duration during earthquakes, and the shape of the 3-D basin, which may cause the seismic response

to differ significantly from that of a 1-D layer (e.g. trapped surface waves). The *S*-wave velocity structure of unconsolidated sediments down to the bedrock, the impedance contrast between these sediments and the bedrock, as well as the shape of the sediment–bedrock interface, can be regarded as the main controlling parameters of such an imprint. Obviously, an exact identification of these parameters is an important step in seismic hazard assessment.

To obtain such detailed models, active *in situ* measurements such as shear wave seismics, surface wave measurements with single stations or arrays, and down-hole and cross-hole techniques can be performed. However, especially in urban areas, it might be difficult to apply these techniques due to the impossibility of making use of explosive sources.

For this reason, non-invasive and cost-effective passive seismic techniques have recently become an attractive option for seismic site effect studies, providing reliable information about the subsurface with a good lateral coverage. Especially over the last decade, environmental noise recordings performed by single station methods to estimate horizontal-to-vertical (H/V) spectral ratios and by 2-D microarray techniques to estimate surface wave dispersion curves have provided very promising results. Among the single-station methods, the Nakamura technique (Nakamura 1989) is most popular. This method allows the estimation of the fundamental resonance frequency of a site in relation to the frequency of the first peak observed in the spectral ratio between the horizontal and vertical components of noise recordings acquired at a single site, which has been confirmed by several studies (e.g. Lermo & Chavez-Garcia 1994; Field & Jacob 1995; Horike *et al.* 2001; Bard & The SESAME project 2004). Tokimatsu & Miyadera (1992) found that the variation of microtremor H/V ratios with frequency corresponds to that of the Rayleigh wave for the *S*-wave velocity profile at the site. Based on a theory for surface (both Rayleigh and Love) waves proposed by Harkrider (1964), Arai & Tokimatsu (2000) presented theoretical formulas for simulating microtremor H/V spectra in which the effects of fundamental and higher modes can be considered. They found that the theoretical H/V spectrum computed for the *S*-wave velocity profile at a site can closely match the observed microtremor H/V spectrum and, vice versa, that the *S*-wave velocity structure at a site can be estimated from the inversion of the microtremor H/V spectrum. Several studies have exploited the availability of measurements of ambient noise to derive a vertical shear wave velocity profile (e.g. Fäh *et al.* 2001, 2003, 2006; Scherbaum *et al.* 2003; Arai & Tokimatsu 2004; Parolai *et al.* 2006).

Soil conditions often vary over relatively short distances. For this reason, recognition of the importance of ground-motion amplification has led to the development of systematic approaches for mapping seismic site conditions (e.g. Park & Elrick 1998; Wills *et al.* 2000; Holzer *et al.* 2005), as well as quantifying both amplitude- and frequency-dependent site amplifications (e.g. Borcherdt 1994). A now standardized approach for mapping seismic site conditions is measuring and mapping v_S^{30}. The Uniform Building Code (International Conference of Building Officials 1997) uses v_S^{30} to group sites into several broad classes, whereas each category is assigned by characteristic factors that can modify the response spectrum in a different way. In fact, many U.S. Building codes (Building Seismic Safety Council 2004) as well as the Eurocode 8 (CEN 2003) now rely on v_S^{30} for seismic site characterization. However, for the sake of comparison with other studies, we will refer in the following to U.S. Building codes only.

Recently, Wald & Allen (2007) presented a method to derive site-condition maps by correlating v_S^{30} measurements with topographic gradient. The basic conclusion of this technique is that the topographic slope from both high- and low-resolution maps might be used as a reliable indicator of v_S^{30} in the absence of geologically and geotechnically based site-condition information because more competent materials, which are characterized by higher seismic velocities, would be more likely to maintain higher gradients, whereas sediments are deposited predominantly in areas with a low gradient. The use of high-resolution data may recover fine-scale variations in the topographic gradient which might better correlate with geological and geomorphic features, although Allen & Wald (2009) found that topographic smoothing (i.e. lower resolution) may provide more stable results.

To check the potential of the previously introduced technique on a local level, the city of Santiago de Chile would be an appropriate test area. In fact, several investigations have been conducted in Santiago de Chile to evaluate site effects (Midorikawa *et al.* 1991; Cruz *et al.* 1993; Toshinawa *et al.* 1996; Bonnefoy-Claudet *et al.* 2009). Pilz *et al.* (2009) compared different site response techniques using both earthquake data and seismic noise analysis. In addition, several data sets that provide geological and geotechnical information, as well as high-resolution topographic data (1 arcsec) are available, showing areas with both low and significant slopes. Furthermore, the city has suffered a significant number of destructive earthquakes in the past, the last one occurring in 1985, with strong intensity variations within the city (e.g., Çelebi 1987). As the modification of strong ground shaking is related to the *S*-wave velocity structure below the site, it is therefore of utmost importance to check if any correlation between the parameters of topographic gradient, v_S^{30}, surface geology, and intensity may exist.

In this work, microtremor measurements in the basin of Santiago de Chile along with available geological and geophysical data are used to derive a 3-D *S*-wave velocity model of the investigated area, which may in turn be used to determine v_S^{30} and for preparation of scenario modelling. First, we give a short overview of the geological conditions and the set-up used for the experiments. Secondly, we show how the *S*-wave velocity model was derived and provide a detailed description thereof, including a comparison with the results of other available data sets. Finally, we test if the slope of topography in the investigated area may provide a reliable proxy for the evaluation of v_S^{30} and therefore be appropriate for site response estimation.

2 GEOLOGICAL SETTING

The city of Santiago de Chile, the country's capital with more than six million inhabitants, lies in the central part of an 80-km-long and 30-km-wide basin, a large bowl-shaped valley at the northern end of the central depression of Chile, which was caused by tectonic movements in the Tertiary of an area between two major faults parallel to two mountain chains running northsouth. Volcanic activity dated between the upper Oligocene and lower Miocene is believed to have formed the basement of the Santiago basin. Its bottom, only indirectly known from gravimetric measurements (Araneda *et al.* 2000), corresponds to an uneven surface unveiled by some buried hill chains that locally outcrop within the basin (e.g. Cerro Renca, Cerro San Cristobal, see Fig. 1). The mapping of the basement topography suggests a large paleo-drainage network associated with small troughs, the deepest one located in the western part of the city. However, more comprehensive data is still missing.

The basin itself is covered by sediments, most of which have been transported from the Andes mountains by a branched river system (Valenzuela 1978). The thickness of the sedimentary cover

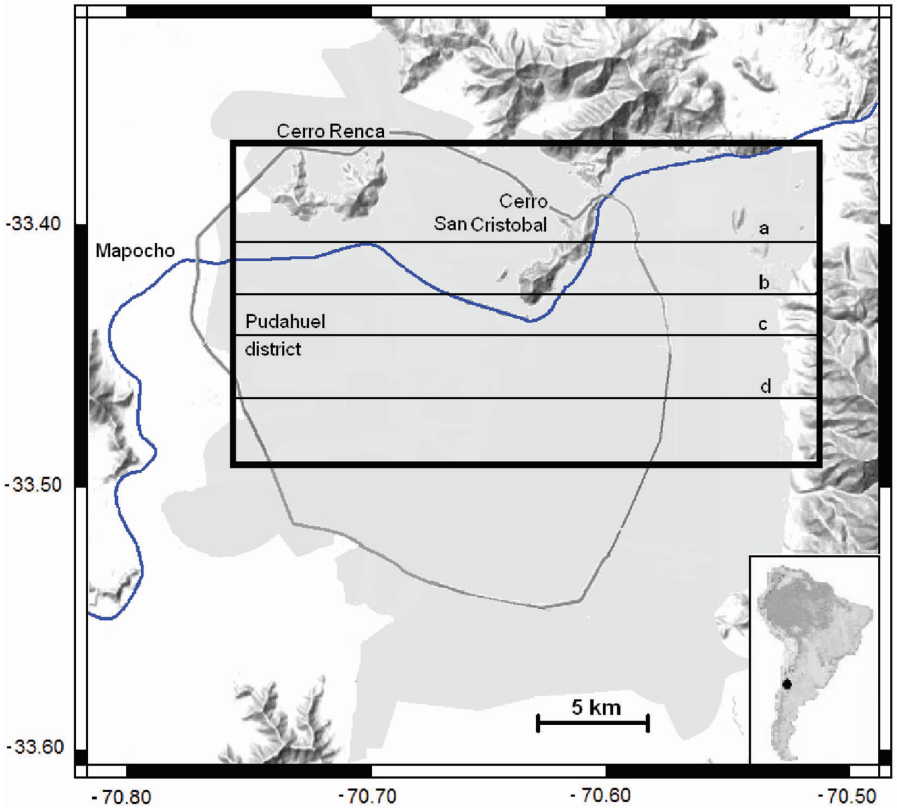

Figure 1. Basin of Santiago de Chile. Areas of high housing density are toned. The highway ring is marked by the dark grey line. The blue line is the Mapocho river. Locations mentioned in the text are indicated. The area of investigation is marked by the black rectangle. Thin lines mark cross-sections shown in Fig. 6.

varies over short scales and can exceed more than 550 m. The sediments are mainly composed of gravel, sand and clay. Some deposits are believed to result from volcanic mud flows or glaciers. Clayey material makes up most of the north-western part of the investigated area. In the eastern part of the basin, large amounts of coarse sediments are associated with the development of the apexes of alluvial fans. A transition zone is found in the centre of the valley. In the south-western part of the investigated area (Pudahuel district), a layer of ash (pumice) is known to sit at the top of the sedimentary column, probably resulting from a major eruption of the Maipo volcano, located 120 km to the southeast, 450 000 years ago (Baize *et al.* 2006). A simplified map of the surface geology is shown in Fig. 2; for further details, see Valenzuela (1978). One must, however, keep in mind that the basin geometry, characterized by sharp lateral and vertical variations of various geological units, is rather complex, resulting in a high level of uncertainty in our current knowledge and has not been mapped in detail so far.

3 DATA ACQUISITION

From May 19 until 2008 June 13, an extensive survey using single-station seismic noise measurements was carried out in the northern part of the city of Santiago de Chile. In total, 146 recordings of ambient noise were carried out (measurement sites shown in Fig. 2) using an EarthData logger PR6–24 instrument connected to a Mark L-4C-3-D sensor with GPS timing. We used sensors with a resonance frequency of 1 Hz and for the digitizer a maximum possible gain (i.e. 10) with which investigation is possible also when H/V peaks are expected to occur down to 0.1–0.2 Hz (Strollo *et al.* 2008a,b). At each site, the signal was recorded with a sampling rate of 100 samples per second for at least 25 min, guaranteeing the statistical stabilization of the signal. Sensor installations were carried out while trying to obtain the best coupling between the instrument and soil and avoiding asphalt. For all measurements, the sensor was protected against wind. On several days, rainfall was slight to moderate, but it has been shown (Chatelain *et al.* 2008) that such factors have no noticeable influence.

4 DATA ANALYSIS

4.1 Deriving H/V spectral ratios

It has already been shown by several studies that H/V spectral ratios provide a reliable estimate of the fundamental resonance frequency of soil deposits. For this purpose, the H/V spectral ratios were computed by dividing the recorded signal into 60 s-long windows and by tapering with a 5 per cent cosine function. As a rule of thumb, it is generally accepted (Bard & SESAME WP02 team 2005; Picozzi *et al.* 2005) that the shortest window length has to be selected in such a way as to include at least 10 cycles of the lowest frequency analysed. Because the thickness of the sedimentary cover can exceed more than 550 m and, therefore, the fundamental frequency is assumed to be low a window length of 60 s can be considered long enough to reliably accomplish the analysis down to a frequency of at least 0.2 Hz. After performing an FFT for each seismometer component and correcting the Fourier spectra for the instrumental response, the amplitude spectra were smoothed using the Konno & Ohmachi (1998) window ($b = 40$) and checked visually for

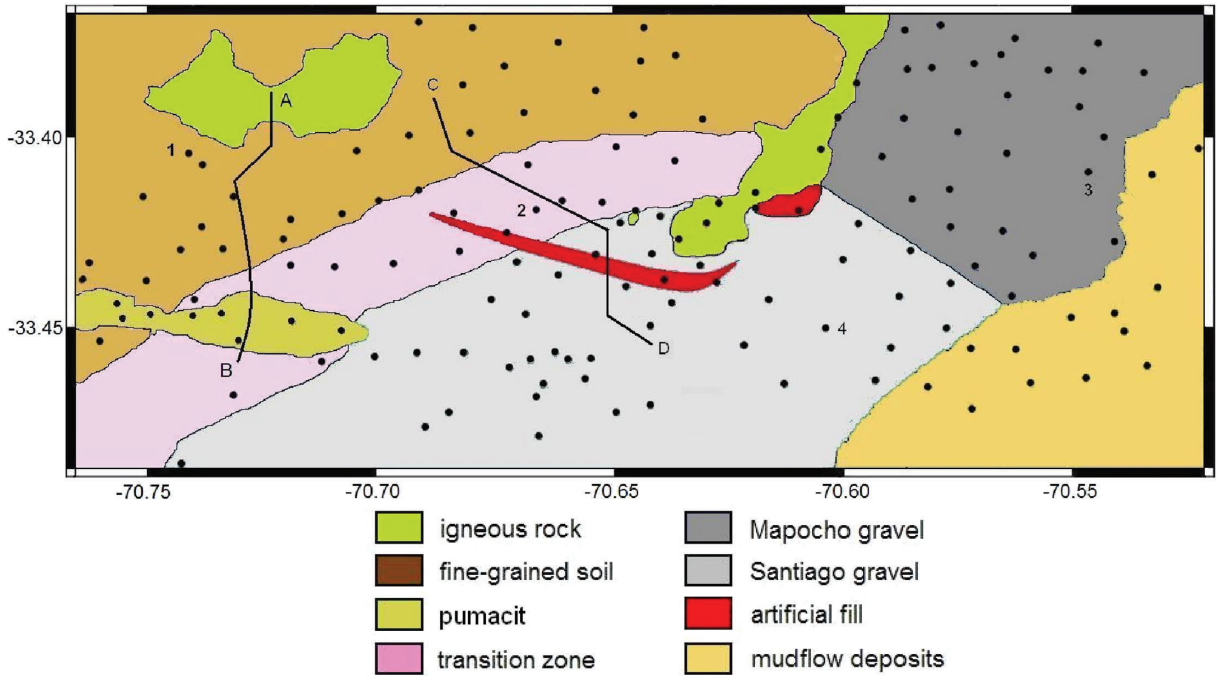

Figure 2. Simplified surface geology of the Santiago basin. Spots indicate the sites where measurements of ambient seismic noise have been carried out. Numbers indicate the locations of the *S*-wave velocity profiles of Fig. 4. Thick lines mark the tracks of the cross-sections shown in Fig. 5.

anomalies between the Fourier spectra of the NS and the EW components. Subsequently, both spectra were averaged (root-mean square) to obtain the horizontal component Fourier spectrum. Afterwards we calculated the spectral ratios between the horizontal and vertical components, and finally we determined the logarithmic mean of all H/V ratios for a given site. For our studies, the number of selected windows (20–30) for this frequency range guarantees stable results (Picozzi *et al.* 2005). The resulting 146 H/V spectral ratios were systematically analysed considering the recommendations proposed by the SESAME consortium (Bard & SESAME WP02 team 2005).

Recordings corresponding to clear and narrow peaks are in great majority located in the northern and western parts of the investigated area (Fig. 3). This suggests the existence of a strong velocity contrast at depth between unconsolidated sediments and the bedrock. On the contrary, flat H/V curves and peaks with low amplitude are mainly found in the southern and eastern parts of the basin where coarser sediments (mainly gravel) outcrop. There, a low impedance contrast between the sediments and the bedrock is likely to exist. Few curves show quite broad peaks; these curves are spread over the entire basin, with no correlation with topographic characteristics and local geology. On the other hand, gravimetric data (Araneda *et al.* 2000) show that at some sites, the thickness of the sedimentary cover varies over short distances. It has been demonstrated (Wooleroy & Street 2002) that broad H/V peaks can occur at sites with large near-surface shear-wave velocity contrasts and a complicated subsurface geometry. Although there might sometimes be difficulties in determining an exact fundamental frequency, these curves can still be used for further analysis since they provide a frequency band of amplification. Considering additional geotechnical site information and site response data obtained from earthquake recordings (see Pilz *et al.* (2009) for further details), the fundamental resonance frequency could be determined for 131 of the 146 measurement sites and is mapped in Fig. 3.

4.2 Inversion of H/V ratios for deriving *S*-wave velocity profiles

We inverted each H/V ratio curve individually under the assumption of a horizontally layered 1-D structure below the site. The H/V ratios are suitable of allowing the effect of Rayleigh and Love waves (also higher modes) to be taken into account. A genetic algorithm forms the basis for the inversion scheme due to the non-linear nature of the problem. The inversion was performed by means of a modified genetic algorithm proposed by Yamanaka & Ishida (1996). In fact, the genetic algorithm allows a non-linear inversion analysis to be accomplished that does not depend upon an explicit starting model and allows the identification of the parameter's search space where the global minimum of the inversion problem is. It has been shown that the shape of H/V ratios around the fundamental resonance frequency and around the first minimum of the average H/V ratio depends mostly on the layering of the sediments (Fäh *et al.* 2001).

Because an infinite number of structural models leading to the same H/V spectrum exist, additional information is needed to constrain the inversion. Several publications (Scherbaum *et al.* 2003; Ohrnberger *et al.* 2004; Parolai *et al.* 2006; Castellaro & Mulargia 2009) show that the H/V inversion can provide reliable results once the total thickness of the sedimentary cover is constrained. For the Santiago basin, the total thickness of the sediments is known from gravimetric measurements (Araneda *et al.* 2000). However, there is some degree of uncertainty in the topography of the bedrock due to the interpolation of the gravimetric data between the measurement sites, which were spaced with an interstation distance of between 500 and 1000 m. Therefore, the total thickness of the sediments was allowed to vary within 10 per cent compared to the estimated value derived by the gravimetric data, allowing us to avoid problems of trade-off between total thickness and the *S*-wave velocity profile and to account for uncertainties.

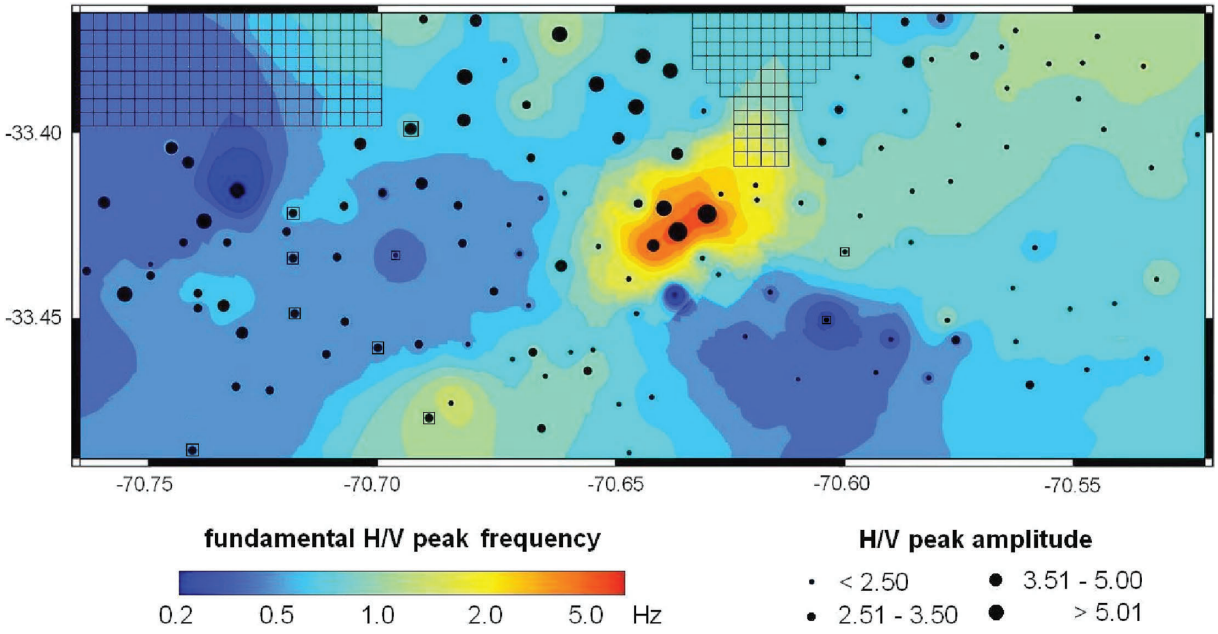

Figure 3. Map of the fundamental resonance frequency of the investigated area. Circles indicate microtremor measurement sites that have been considered for interpolation. Spots enclosed by squares represent broad H/V peaks (see text for further discussion). Diameter of the spots corresponds to H/V peak amplitude. In the hatched area, no measurements were carried out; hence results are only due to interpolation.

For the inversion, the velocity ranges of the layers were fixed to wide ranges by considering the value intervals for the different sediments in the Santiago basin given by Bravo (1992), Lagos (2003) and Ampuero & Van Sint Jan (2004). In addition, we made use of detailed stratigraphic information derived from about 150 boreholes distributed over the entire investigated area with depths ranging between 20 and 300 m (predominantly around 100 m) drilled by the Chilean water company Aguas Andinas S.A. for the determination of the groundwater level. It has been shown (e.g. Arai & Tokimatsu 2004) that sediment thickness and *S*-wave velocity have the most significant effects on the H/V spectrum, whereas the influence of other parameters such as density (for inversion, layer parameters were taken from Valenzuela 1978 and fixed) and *P*-wave velocity is much smaller. Hence, for calculating the *P*-wave velocity, the relationship of Kitsunezaki *et al.* (1990) was used: v_p (m s^{-1}) = 1.11 v_s (m s^{-1}) + 1290.

The initial starting population (50 individuals) is generated by a uniform random distribution within the entire parameter space. Throughout this study, the number of layers was prescribed (generally seven, four if the sedimentary cover thickness is below 50 m). As needed for the computation of the H/V spectral ratios, a fixed standard structural model for the bedrock layer with a high velocity up to 2500 m s^{-1}, according to Ortigosa & Lástrico (1971) and confirmed by Bravo (1992), and a density of 2.6 t m^{-3} (Araneda *et al.* 2000) was used. Because this inversion is a kind of probabilistic approach using random numbers for finding models near the global optimum solution, the inversions are repeated several times, varying the initial random number.

An example is shown in Fig. 4, which presents the results of the inversion analysis and the fit of the calculated to observed H/V ratio curves. The presented *S*-wave velocity profiles provide a rough overview of different velocity structures that are found in the investigated area. We note that the calculated H/V curves fit the observed values well. The reliability of the inversion results is influenced not only by the quality of the input data, but also depends on the frequency range of the H/V curve. However, deeper parts of the model are more influenced by the trade-off between parameters (Scherbaum *et al.* 2003) and are therefore characterized by a higher uncertainty. This is also confirmed by larger instabilities in the *S*-wave velocity profiles characterized by misfits within +10 per cent of the best model with depth. Although the resolution for deeper parts of the model remains lower, it is still possible to retrieve an average *S*-wave velocity, which might be sufficient for engineering seismology purposes. In addition, the fact that for more than 85 per cent of all profiles the total depth of the sedimentary cover differs by only a few percent from the value provided by the gravimetric data set (i.e. the inversion does not provide a value at the margin of the parameter range of the sedimentary cover thickness) confirms the reliability of the underlying gravimetric data.

For validation of the inversion results, we compared the calculated *S*-wave velocity profiles with other studies (Bravo 1992; GeoE-Tech 2007) in which local velocity information for a few single sites derived from refraction measurements down to a maximum of 30 m is described. Although details about the velocity structure in the uppermost parts of the Santiago basin cannot be retrieved by our inversion technique as the resolution is not high enough for these layers and, therefore, only information about the average *S*-wave velocity can be retrieved, the average *S*-wave velocities of these studies are consistent with our data (deviations between values are at most 20 per cent, often below 10 per cent).

Although Pilz *et al.* (2009) found reliable H/V peaks for 131 of 146 measurement sites whereas, on the other hand, it is almost impossible to retrieve a reliable *S*-wave velocity profile for an almost flat H/V curve, in the end only 125 measurements were suitable for performing an inversion procedure. Only these profiles were used for further analysis.

4.3 Interpolation of the Santiago basin *S*-wave velocity model

Each of the 125 local *S*-wave velocity profiles derived from the H/V inversion was then re-sampled with a spatial resolution of 1 m,

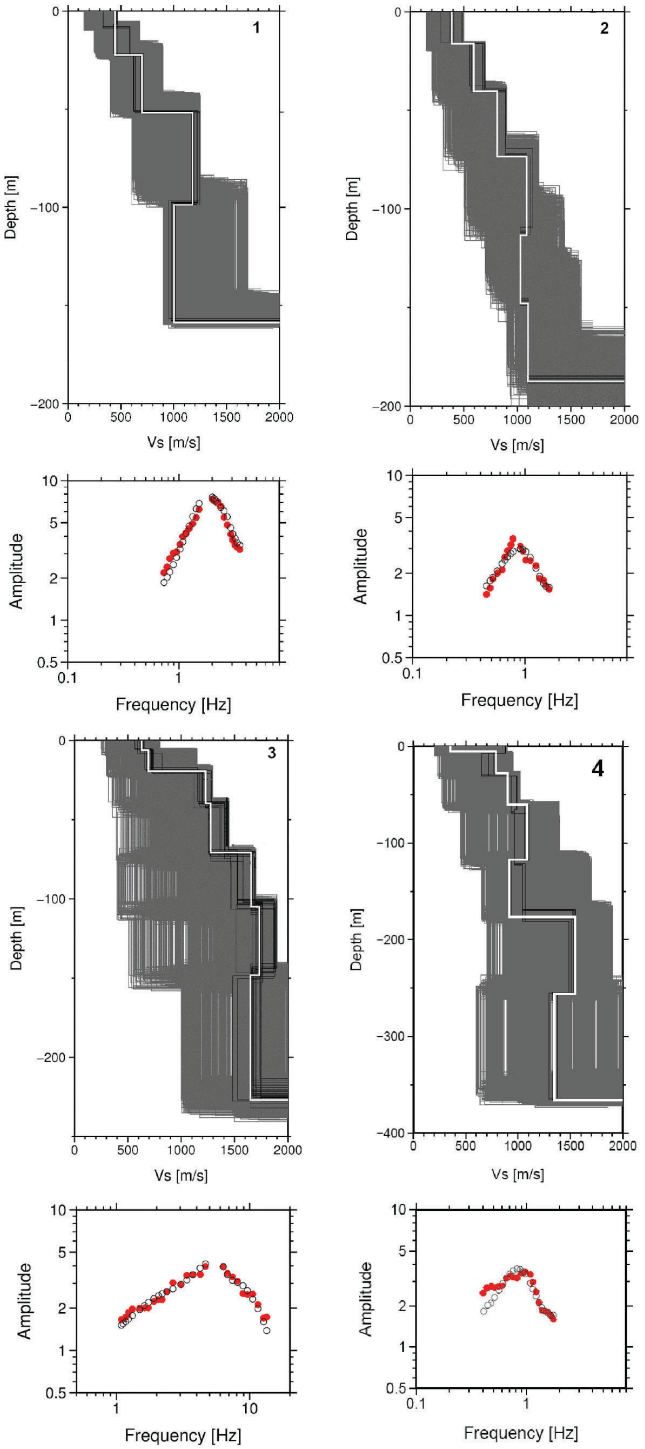

Figure 4. Examples of the inversion results and fits to the H/V spectral ratio curves. Top panel: All four figures show all tested models (grey lines), the minimum misfit model (white line), and all models lying within the minimum misfit + 10 per cent range (black lines). Bottom panel: Observed H/V ratio (red dots) and the H/V ratio for the minimum misfit model (open black circles). Numbers indicate sites where the measurements have been carried out and are shown in Fig. 2.

and a 3-D *S*-wave velocity model, parameterized by a rectangular grid with a spatial horizontal resolution of 100 m, was derived. The model contains a detailed description of the sedimentary basin shape derived from gravimetric data as defined by the contact between the lower *S*-wave velocity sediments and higher *S*-wave velocity bedrock. We incorporate orography, that is the shape of the surface, based on digital elevation model data, which are available with a resolution of 1 arcsec (approximately 30 m) for all of Santiago.

Different methods have been proposed for the interpolation of spatially changing natural properties (e.g. Isaaks & Srivastava 1989; Wackernagel 1998). A popular method based on an irregularly distributed spatial data set was introduced by Krige (1951). This method uses the local estimation of a parameter based on the weighted spatial mean of samples in the neighbourhood. The weights are defined not only by the distance, but also by the spatial distribution of the samples. Therefore, the accuracy of the estimation depends both on the number of samples and their spatial distribution. A major advantage of the kriging method is the prevention of nugget effects that might occur when dealing with unevenly distributed data. We used a simple ordinary kriging (i.e. the estimation of means in a moving neighbourhood, see Wackernagel 1998 for details) technique which often shows a performance as good as, or even better than, more complex co-kriging methods (Goovaerts 2000) and spline approximations, which are only special cases of the general kriging problem (Laslett 1994).

The performance of the interpolation technique was tested using cross validation (Isaaks & Srivastava 1989). The idea consists of removing one *S*-wave velocity profile observation from the input data and to re-estimate its value from the remaining data with the help of the described algorithm. The comparison criterion is the mean square error between the former *S*-wave velocity profile and its re-calculated estimate. The value should be close to zero if the interpolation algorithm is accurate. The procedure is repeated until every sample has been, in turn, removed. The cross validation of this particular form is therefore suitable for assessing the interpolation scheme because the reliability of the interpolation in undersampled areas can be verified. Of course, larger variations appear when removing one profile close to the edge of the investigated area because the lower number of surrounding profiles cannot compensate for the missing data. In general, however, when removing one profile, the mean error between the interpolated *S*-wave velocity and the values estimated by the inversion algorithm is usually below 10 per cent; only for the south-western area differences are higher (up to 22 per cent). We also found that our *S*-wave velocity model is stable both for *S*-wave velocity values close to the surface and for deeper parts of the basin. Due to large discrepancies at the edge of the area of investigation, we therefore refrained from interpolating the *S*-wave velocity outside an area limited by a linear connection between the outermost sites. By reason of the spatial distribution of the measurements, we could fit the *S*-wave velocity within a lateral extent of around 270 km^2.

5 CHARACTERISTICS AND INTERPRETATION OF THE *S*-WAVE VELOCITY MODEL

To determine the validity of the interpolated model, we first compared cross-sections of our model with available geological cross-sections from the literature (Bravo 1992; Iriarte 2003; Iriarte *et al.* 2006; Pasten 2007), although the link between stratigraphy and *S*-wave velocity is not expected to be direct due to velocity variations that occur with the different kinds of lithology. In all of these studies, the geological units have only been drawn for the uppermost 100–150 m with large lateral uncertainties, especially for deeper parts. As an example, Fig. 5 shows a comparison of two geological

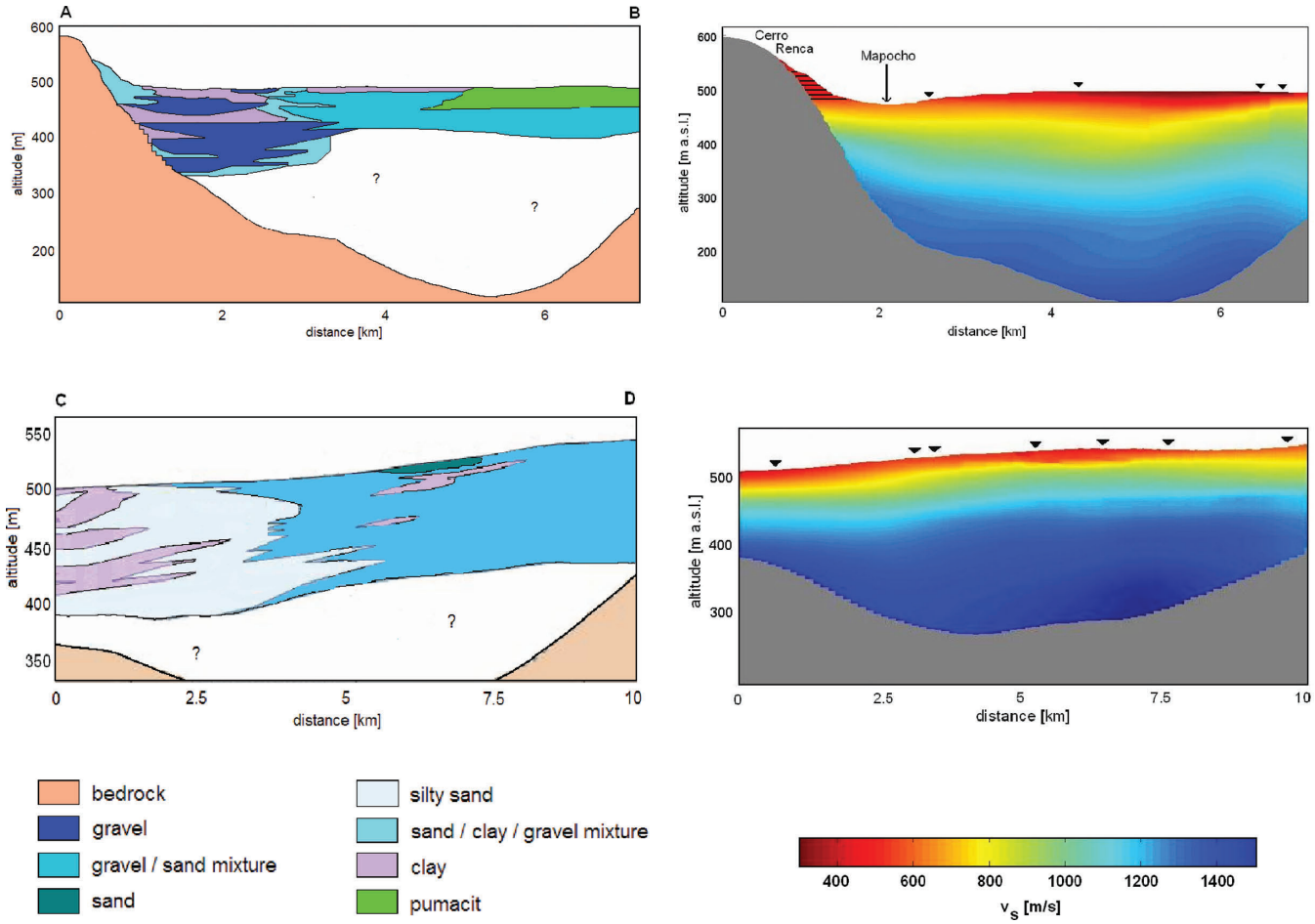

Figure 5. Left panel: Geological cross-sections along profiles A-B (upper) and C-D (lower) marked in Fig. 2 after Iriarte (2003). Right panel: The corresponding 2-D *S*-wave velocity models calculated by means of interpolating between single *S*-wave velocity profiles. Black triangles mark the location of the measurement sites within a distance of 500 m to the cross-section. For the striped part in the velocity cross-section A-B, the results are only due to interpolation.

and the corresponding interpolated *S*-wave velocity cross-sections. It must be mentioned that the geological profiles, presented in different publications, are based on different data sets. Therefore, and due to the large uncertainties, differences in the geologic units of Figs 2 and 5 need to be explained.

In the southern (i.e. right) part of cross-section A-B, the layer of pumacit, characterized by a rather low *S*-wave velocity, is clearly visible. Our model also shows higher velocities just below the surface for the northern (i.e. left) part of this cross-section, an area mainly composed of gravel. Differences in orography between both profiles are due to the different data sets; for the interpolated *S*-wave velocity model we used data with a high resolution of one arcsec, enabling us to illustrate topographic details like the riverbed of the Mapocho which is cut into the sediments, clearly visible to the left of cross-section A-B. For the submontane part of Cerro Renca, the calculated *S*-wave velocity is only based on interpolation because no measurements have been carried out in the vicinity. Hence, the results cannot be considered to be reliable and are therefore masked in Fig. 5. In profile C-D, the higher velocities of the gravel-sand body, as well as the lower velocities of the sand layer can easily be identified. Therefore, although our model cannot resolve geological details, a general agreement between both is found, allowing us to reliably point out local characteristics that are shown or only foreshadowed in other geological data sets.

Additional cross-sections of our velocity model of the Santiago basin are shown in Fig. 6. As expected, all profiles show a trend of increasing *S*-wave velocities with depth, but differences in the velocity gradient can clearly be seen, even at a first glance. However, strong lateral variations can be justified. Figs 6a and b show that to the east of Cerro San Cristobal, the *S*-wave velocity is higher than to the west. As already mentioned and also reported in Bonnefoy-Claudet *et al.* (2009) and Pilz *et al.* (2009), flat H/V curves and H/V spectral ratios of low amplitude are mainly located in the eastern parts of the basin over dense sediments, that is Santiago and Mapocho gravel. Up to now it has been assumed that these parts of the basin are characterized by the high seismic velocities of the sediments leading to small velocity contrasts with the bedrock. Our results strongly support this assumption, as well as the distinction between Santiago gravel and Mapocho gravel, as proposed by to Valenzuela (1978) and in contradiction to Baize *et al.* (2006). The latter one, located in the northern part of the investigated area (Fig. 2), is characterized by higher compactness resulting in higher velocities. Likewise, Fig. 4 shows higher *S*-wave velocities for profile 3 (Mapocho gravel) than for profile 4 (Santiago gravel). In addition, the *S*-wave velocity for the gravel body is increasing slightly faster in Fig. 6a (around 70.55°W) than in Fig. 6c (between 70.55 and 70.60°W).

The sub-surface extension of the gravel body is only known approximately and only for the uppermost part with the help of a

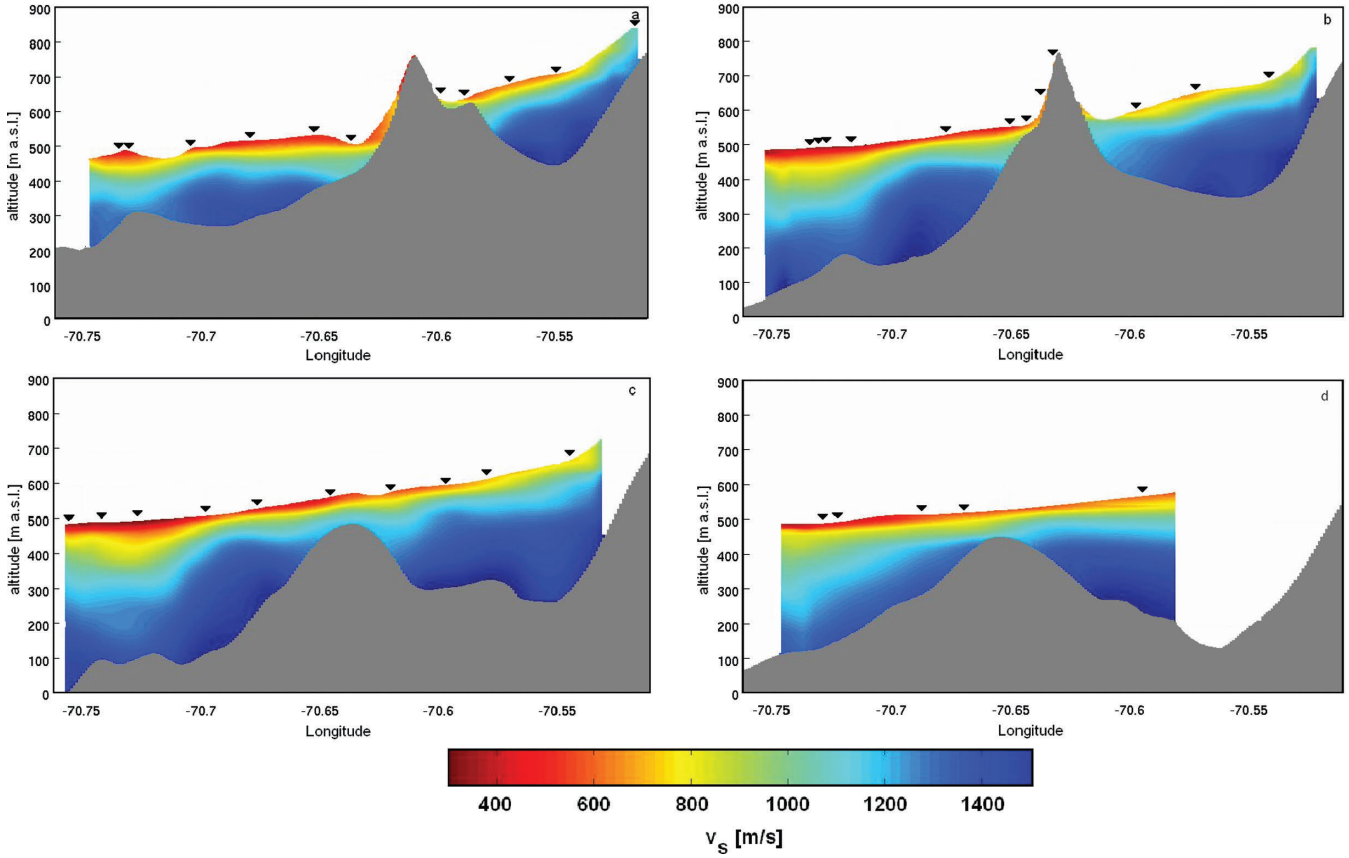

Figure 6. Westeast cross-sections of the interpolated 3-D *S*-wave velocity model within the area of investigation. Locations of the profiles are indicated in Fig. 1. Black triangles mark measurement sites within a distance of 500 m to the cross-section. (a) Lat 33.405°S, (b) Lat 33.425°S, (c) Lat 33.440°S and (d) Lat 33.465° S. For all profiles, topography is exaggerated about 16 times. The shape of the bedrock, shown in grey pattern, is derived from gravimetric data. Orography is based on high-resolution digital elevation data.

few boreholes. It has been assumed that the entire gravel body is prograding to the northwest below the fine series, which is also supported by our model. Fig. 6b shows relatively high *S*-wave velocities for the lowermost 200 m of the sediments between 70.67 and 70.70°W.

To the west of the investigated area (Pudahuel district, see Fig. 1), the thick layer of pyroclastic flow deposits, outcropping at the top of the filling and characterized by a *S*-wave velocity being well below the velocity of the surrounding materials, can clearly be seen (Fig. 6c). Furthermore, the assumption made by Baize *et al.* (2006) that this low-velocity layer continues at depth towards the south as it may have resulted from a single eruptive phase of the Maipo volcanic complex can be verified. Also, our basin model shows that south of 33.45°S (Fig. 6d) the velocities for the topmost 150–200 m of sediments are lower compared to the northern part. The shape of this sequence was previously not imaged in detail.

In general, our model is able to reliably point out local characteristics shown in other data sets, but takes advantage of the fact that all individual *S*-wave velocity profiles reach the bedrock albeit the resolution for deeper parts of the model remains lower. Furthermore, all recent publications (Baize *et al.* 2006; Pasten 2007; Bonnefoy-Claudet *et al.* 2009) distinguish only three soil categories: gravel, fine deposits and ashes for the Santiago basin, claiming that only these categories behave differently from each other under seismic excitation. We showed that this simplification does not hold as strong lateral *S*-wave velocity differences, even within the single units, occur and therefore also no simple depth—*S*-wave velocity relation, as suggested by Bravo (1992) and Pasten (2007), may exist. Furthermore, the complexity of the lithological succession, characterized by sharp lateral and vertical variations of the physical properties and of the *S*-wave velocity gradient over short scale, may even hint that not only depositional processes, but also tectonic activity accounts for this complexity.

6 COMPARISON OF SLOPE OF TOPOGRAPHY, *S*-WAVE VELOCITY, AND MACROSEISMIC INTENSITY

6.1 Correlation between slope of topography and v_S^{30}

As our model can provide reliable information about the *S*-wave velocity structure of the basin, and topographic data for the entire basin are available at a high resolution, we checked if a simple and inexpensive technique suggested by Wald & Allen (2007), based on a supposed correlation between the slope of topography and the surficial *S*-wave velocity, exists and might be useful for soil classification in Santiago de Chile.

We first calculate the slope of the topography for the entire area under investigation. As the elevation in the Santiago basin steadily increases slightly from west to east, with only a marginally rising gradient, most of the investigated area is characterized by a gentle slope gradient less than 0.03 (i.e. vertical rise over horizontal distance traversed; Fig. 7). Extended hills like Cerro Renca and Cerro

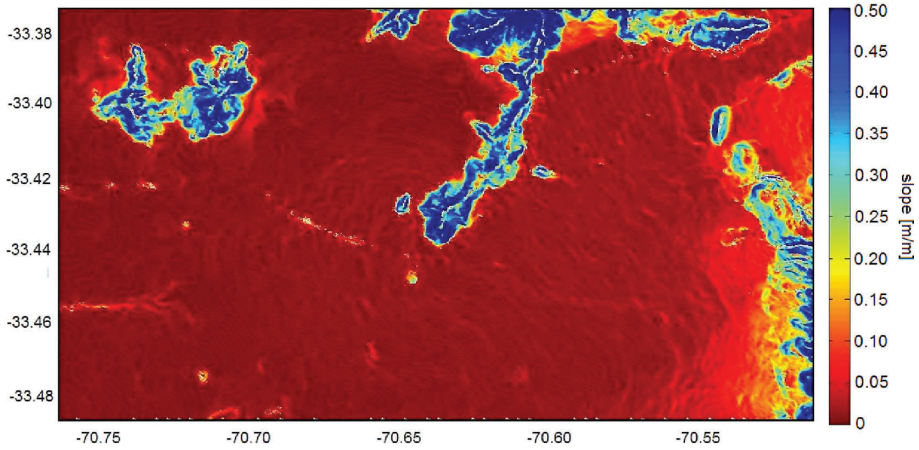

Figure 7. Topographic gradient of the area under investigation, calculated using a topographic resolution of 1 arcsec.

San Cristobal outcropping from the sedimentary filling and characterized by steep slopes can easily be seen, while even the riverbed of the Mapocho can be identified.

To compare the topographic gradient with v_S^{30} values, we choose to characterize the relationship in terms of discrete steps in *S*-wave velocity according to the U.S. National Earthquake Hazards Reduction Program (NEHRP) (Building Seismic Safety Council 2004). To increase resolution, the NEHRP boundaries are further subdivided into narrower velocity ranges, following Wald & Allen (2007).

As it is our aim to verify if any correlation between slope and v_S^{30} exists using data collected on a local scale, we first re-calculated the slope ranges for the associated v_S^{30} ranges for a topographic resolution of 1 arcsec using the technique described in Wald & Allen (2007). Results are listed in Table 1. Although the limited number of only 125 measurement sites will allow only a rough estimation of the correlation coefficients, tendencies should be verifiable. Although large parts of the Santiago basin are characterized by slope values not differing too much from each other, the scatter in the resulting v_S^{30} is high. Hence, no correlation between high-resolution slope information and v_S^{30} can be seen in Fig. 8, although the tendency in Table 1 shows on average an increment of the coefficients with slope.

Of course, the application of lower resolution topographic data will result in slope values differing from the ones given in Allen & Wald (2009). Their results, based on a topographic resolution of 9 arcsec, are also listed in Table 1. However, this extreme divergence cannot completely be explained by the fact that we used high-resolution topographic data. In fact, when using a lower resolution of 9 arcsec or even 30 arcsec for calculating the topographic gradient at each measurement site, as suggested by Allen & Wald (2009), steep slopes over short distances will not be resolved due to the lower sampling rates inherently smoothing maximum slope values inferred from the topography (Fig. 8b). We note that the measured v_S^{30} values are still much higher than expected. Only for steeper slopes an agreement with the given velocity range is found. The expected trend that materials characterized by high velocities are more likely to maintain steep slopes and vice versa can only benevolently be seen. But on the other hand, when using a lower resolution, high slope values (approximately greater than 0.1) will tend to be scaled down, which can also be seen when comparing Figs 8a and b, leading to even less agreement. Hence, independent of the spatial resolution used, our results reduce any confidence in the applied correlations between topographic gradient and v_S^{30}. Even lower resolution data (30 arcsec) does not provide comparable estimates of v_S^{30}, although the relief in the Santiago basin is quite low.

However, studies dealing with estimating local site conditions mainly focus on densely populated areas with a moderate extension. Therefore, it is of utmost necessity to find a technique giving a reliable overview over regional scales, which can be applied with confidence on a local scale. At least to reduce the overall bias for Santiago de Chile, a general shift to lower slope–v_S^{30} correlation values would therefore be necessary. But in contrast, Wald & Allen (2007) observed exactly the opposite trend for the Salt Lake City region. Therefore, it seems that a general rule cannot be found.

Table 1. v_S^{30} and associated topographic slope ranges calculated according to Wald & Allen (2007) from measurements carried out in Santiago de Chile for a topographic resolution of 1 arcsec and taken from Allen & Wald (2009) for active tectonic regions using a 9 arcsec resolution data set.

NEHRP site class	v_S^{30} range (m s^{-1})	Slope range calculated from measurement data	Slope range given by Allen & Wald (2009)
D	180–240	no values	0.00030–0.00035
	240–300	no values	0.00035–0.010
	300–360	<0.0085	0.010–0.024
C	360–490	0.0085–0.013	0.024–0.08
	490–620	0.013–0.033	0.08–0.14
	620–760	0.033–0.096	0.14–0.20
B	>760	>0.096	>0.20

Note: Only NEHRP v_S^{30} ranges found in the Santiago basin are listed here.

6.2 Correlation between *S*-wave velocity and macroseismic intensity of the 1985 Valparaiso event

The reason for the apparent lack of coincidence in any correlation between v_S^{30} and the topographic slope might be clarified when analysing the geological situation. A large part of the Santiago basin is characterized by a low, but measurable topographic gradient with only a limited number of outcropping bedrocks characterized by steep slopes (Fig. 7). In contrast, the surface geology is rather heterogeneous (Fig. 2), indicating that the deposition played a minor role in differentiating the material and their friction angles. Therefore, one might check if a first-order correlation between v_S^{30} and surface geology may be detectable. To this regard, we mapped v_S^{30} for the area under investigation using a 2-D kriging algorithm similar to the one described in Section 4.3. Again, we calculated v_S^{30} only

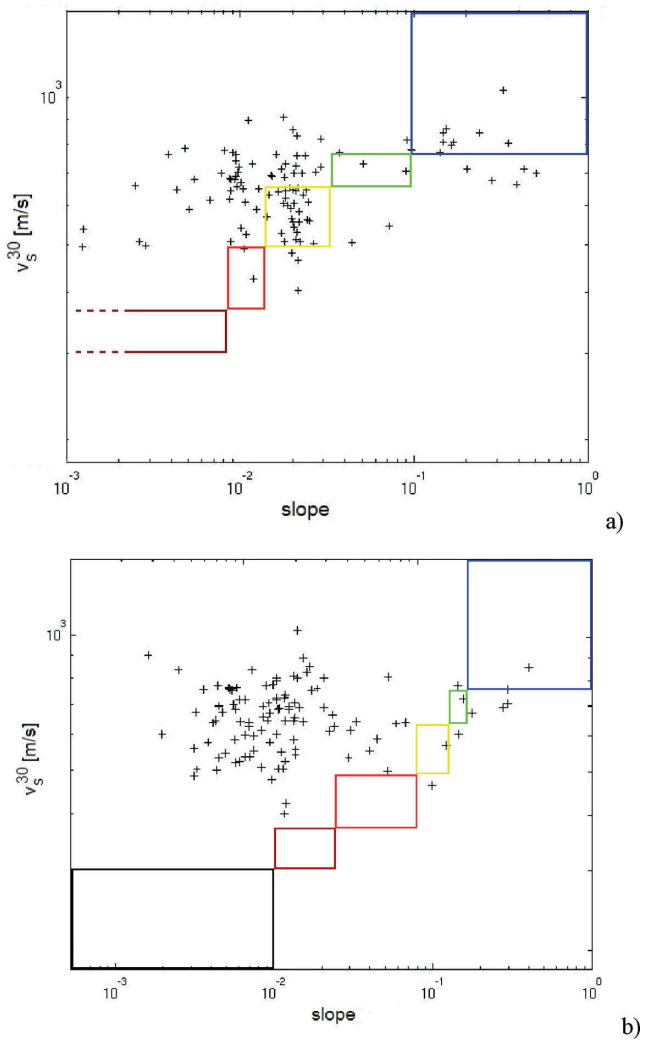

Figure 8. Correlation of measured v_S^{30} against slope of topography for different resolution. Color-coded polygons represent v_S^{30} values and their associated slope ranges listed in Table 1. Top panel: Topographic resolution of 1 arcsec and the resultant calculated slope ranges. Bottom panel: Topographic resolution of 9 arcsec. Values of associated slope ranges are taken from Allen & Wald (2009) for active tectonic regions. See text for further discussion.

for an area limited by a linear connection between the outermost measurement sites. Results are shown in Fig. 9.

Areas characterized by different *S*-wave velocities in the uppermost 30 m can clearly be identified. In the western part, an ellipsoidal area of low v_S^{30} values represents the layer of pumacit on the top of sedimentary filling (Fig. 2). In the central part, the outcropping igneous bedrock of the Cerro San Cristobal is apparent. The v_S^{30} values found there contrast with those in the surroundings and depict the shape of the hill quite well. Note that in the northern part of the Cerro San Cristobal and also close to the Cerro Renca, no ambient noise measurements have been carried out. Therefore, no reliable v_S^{30} interpolation values are found for these parts of the investigated area and are thus masked out in Fig. 9.

Some individual measurement sites in the central and the north-eastern part show low v_S^{30} values located on gravel where higher velocities would have been expected. These differences confirm that within the same lithology strong lateral variations of *S*-wave velocity can be found. The changes are explainable when bearing in mind the course of the Mapocho as it is drawn in Fig. 1. In accordance with Pasten (2007), the river beds in the Santiago basin and the associated flow velocity are mainly controlled by topography. As a result, where the flow velocity is low sediment drops out of the flow and deposits. Therefore, this emphasises that geology-based values should not be taken as constants within a specific geological unit as changing material properties (e.g. particle size) often appear.

When comparing our v_S^{30} map with the MKS intensity values determined for the $M\mathrm{w} = 7.8$ (epicentre 120 km west of Santiago) earthquake of 1985 March 3 (Astroza & Monge 1991; Fig. 10) it can be seen that the intensity distribution for that event was mainly influenced by local variations of v_s. Most of the damages was concentrated in the north-western part of the city where a small-sized low-quality building stock can be found (Astroza *et al.* 1993). At first glance, this cannot be explained by an accordance of the fundamental resonance frequencies of the soil and the building stock. Theoretical height–period relationships suggest that small-sized structures in that area might have a natural frequency of more than 5 Hz whereas the fundamental frequency of the soil is well below 1 Hz (Fig. 3) but one should keep in mind that higher harmonics also might correspond to the eigenfrequency or even to higher harmonics of these buildings.

However, there is a slight tendency that large H/V peak values are observed in areas with higher intensities (western part of the city) and small H/V peak values in areas with lower intensities (eastern part). Measurements carried out on Cerro San Cristóbal, showing high fundamental frequencies and high H/V peak amplitudes, do not follow this trend. Nonetheless, a more detailed analysis is not possible. On top of the pumacit layer, where the intensity reached a maximum, the lowest v_S^{30} values are found (Fig. 9) but, in contrast, only some H/V ratios show high amplitudes. The highest H/V peak amplitudes are found for the central northern part of the investigated area (Fig. 3). Summarizing, considering the outlined results, a direct correlation between H/V amplitude and damage is found. This result is not surprising since damages depend on ground motion intensity but also on building vulnerability.

The eastern part of the investigated area shows the highest v_S^{30} and low-intensity values. Of course, only a general trend can be identified when mapping v_S^{30} and no strict borders should be drawn between individual units. Also Pilz *et al.* (2009) found different standard spectral ratio amplitudes for their seismic network at sites within the same v_S^{30} range, indicating the incompleteness of v_S^{30} to fully describe site effects and building vulnerability and the need to consider additional parameters. When comparing Figs 2, 7 and 10, it seems obvious that, except for the outcropping of igneous bedrock, no clear correlation between evaluated intensities and topographic slope can be found for the 1985 event. The surface geology offers a very poor first-order indication of intensity distribution whereas v_S^{30} might allow a better, although only approximate, distinction of areas characterized by different intensity values. Of course, v_S^{30} is not the only factor controlling ground-motion amplification. In addition, to topographic effects mentioned in the introduction, 2-D and 3-D effects of deep sedimentary basins can also modify the observed level of ground shaking.

7 CONCLUSIONS

The investigation carried out in this work has shown that it is possible to derive a reliable model of the *S*-wave velocity structure for the basin of Santiago de Chile by means of low cost

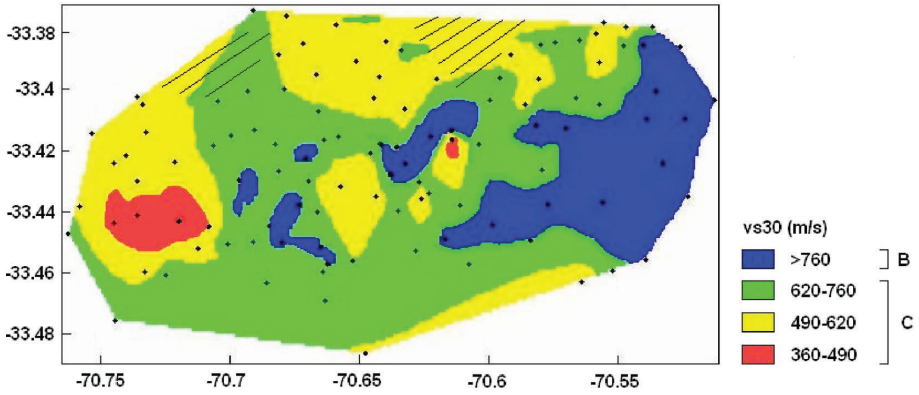

Figure 9. v_S^{30} (NEHRP classification) for the area limited by a linear connection between the outermost measurement sites. Black dots show the location of the ambient noise measurement sites used for mapping v_S^{30}. In the dashed area, no measurements were carried out. Therefore, the results are only due to interpolation and are not plausible as outcropping bedrock can be found there.

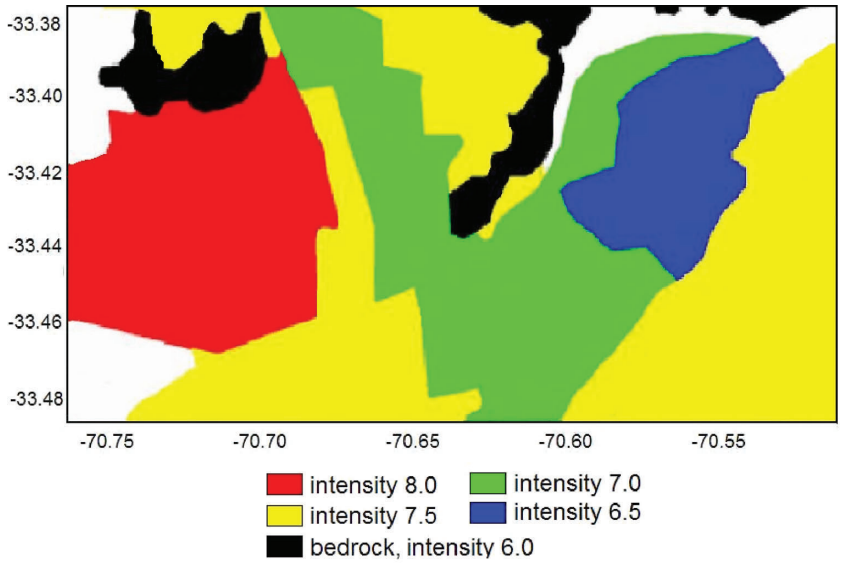

Figure 10. Intensities (MSK scale) for the 1985 earthquake of the investigated area. Values are taken from Astroza & Monge (1991). In the white parts, no reliable intensity values could be determined due to the limited amount of information available.

measurements of ambient seismic noise. Our results are consistent with other available data sets.

One hundred and forty-six measurements of seismic noise were carried out in the city of Santiago, of which 125 allowed further analysis as a confident estimate of the fundamental resonance frequency at these sites was possible. Calculated H/V spectra were systematically inverted under the assumption of a horizontally layered 1-D structure using geotechnical data and knowledge of the thickness of the sedimentary cover, which has been determined previously by gravimetric measurements. This enabled us to derive *S*-wave velocity profiles for each measurement site, which formed the basis for a 3-D *S*-wave velocity model for the entire investigated area with the help of a kriging algorithm. Comparison of our results with existing velocity profiles gained by seismic refraction experiments and additional geological data shows good agreement. We found quite different *S*-wave velocity–depth gradients within the Santiago basin, indicating the impossibility of finding a simple relation between both parameters. However, the resolution of our model could be improved by adding more measurement sites.

As inexpensive and simple techniques for deriving local site response and amplification are of broad interest, we tested if a simple relationship between the slope of the topography and v_S^{30} exists on a local scale. Because no simple correlation between the topographic gradient and surficial geology (i.e. fast and more competent material indicating steeper slopes) exists in the investigated area, no linkage between slope and v_S^{30} could be found due to rather high *S*-wave velocities appearing in the Santiago basin, regardless of which spatial resolution is used. Although the investigated area is characterized by low and steep slope values it is not possible to establish a rough estimation for site amplification based on topographic gradient. On the contrary, a better but still only approximate correlation between v_S^{30} and local geological conditions is visible. A higher resolution of the v_S^{30} map may, of course, be accomplished by adding more measurement sites. Further proof serves when taking into account the distribution of the observed intensities of the 1985 Valparaiso event, which are clearly influenced by the v_S^{30} distribution and cannot, even at a rudimentary level, be derived from the topographic gradient.

In addition to near-surface site conditions, seismic waves are also known to be influenced by sediment thickness and basin structure. During the next phase of this project, we will therefore make use of our knowledge so far acquired and use the established model of

the basin of Santiago de Chile as a basis for realistic modelling of seismic wave propagation. In the end, this will lead to the calculation of seismic hazard scenarios.

ACKNOWLEDGMENTS

This work was supported by the Helmholtz research initiative 'Risk Habitat Megacity'. We are grateful David Solans, Natalia Silva and José Gonzalez for assistance during the field work. Instruments were provided by the Geophysical Instrumental Pool Potsdam. Many thanks to Magdalena Scheck-Wenderoth for discussions about the basin structure and the tectonic implications. The comments of Francisco Sánchez-Sesma, David Halliday and of an anonymous reviewer improved the paper and are gratefully acknowledged. Kevin Fleming kindly revised our English.

REFERENCES

Allen, T.I. & Wald, D.J., 2009. On the use of high-resolution topographic data as a proxy for seismic site conditions (v_s^{30}), *Bull. seism. Soc. Am.,* **99,** 935–943.

Ampuero, A. & Van Sint Jan, M., 2004. Velocidades de onda medidas en Santiago con el ensayo de refracción sísmica, *5th Congreso Chileno de Ingeniería Geotécnica*, Universidad de Chile, Santiago, Chile.

Arai, H. & Tokimatsu, K., 2000. Effects of Rayleigh and Love waves on microtremor H/V spectra, in *Proceedings of the 12th World Conference on Earthquake Engineering,* paper 2232.

Arai, H. & Tokimatsu, K., 2004. S-wave velocity profiling by inversion of microtremor H/V spectrum, *Bull. seism. Soc. Am.,* **94,** 53–63.

Araneda, M., Avendano, F. & Merlo, C., 2000. Gravity model of the basin in Santiago, Stage III, in *Proceedings of the 9th Chilenian Geological Congress,* **2,** 404–408.

Astroza, M. & Monge, J., 1991. Seismic microzones in the city of Santiago. Relation damage-geological unit, in *Proceedings of the Fourth International Conference on Seismic Zonation,* Stanford, CA, USA, 595–599.

Astroza M., Moroni, M. & Kupfer, M., 1993. Calificación sísmica de edificiosde albañilería de ladrillo confinada con elementos de hormigón armado, *Memorias de las XXVI Jornadas Sudamericanas de Ingeniería Estructural,* **1,** Montevideo.

Baize, S., Rebolledo, S., Lagos, J. & Rauld, R., 2006. A first-order geological model of the Santiago basin, in *Proceedings of the Conference on 1906 Valparaíso Earthquake Centennial,* paper NGT1–05.

Bard, P.Y. & Bouchon, M., 1985. The two-dimensional resonance of sediment filled valleys, *Bull. seism. Soc. Am.,* **75,** 519–541.

Bard, P.Y. & The SESAME project, 2004. An overview and main results, in *Proceedings of the 13th World Conference on Earthquake Engineering,* Vancouver, Canada, Paper 2207.

Bard, P.Y. & SESAME WP02 team, 2005. Guidelines for the implementation of the H/V spectral ratio technique on ambient vibrations—measurements, processing and interpretations, *European Comission – Research General Directorate Project No. EVG1-CT-2000–00026 SESAME,* D23.12.

Bielak, J., Xu, J. & Ghattas, O., 1999. Earthquake ground motion and structural response in alluvial valleys, *J. Geotech. Geoenviron. Eng.,* **125,** 413–423.

Borcherdt, R.D., 1994. Estimates of site-dependent response spectra for design (methodology and justification), *Earthquake Spectra,* **10,** 617–654.

Bouchon, M., 1973. Effects of topography on surface motion, *Bull. seism. Soc. Am.,* **63,** 615–622.

Bravo, R.D., 1992. Estudio geofisico de los suelos de fundación para un zonificacion sísmica del area urbana de Santiago Norte, *PhD thesis*. Universidad de Chile, Santiago, Chile.

Bonnefoy-Claudet, S., Baize, S., Bonilla, L.F., Berge-Thierry, C., Pasten, C.R., Campos, J., Volant, P. & Verdugo, R., 2009. Site effect evaluation in the basin of Santiago de Chile using ambient noise measurements, *Geophys. J. Int.,* **176,** 925–937.

Building Seismic Safety Council (BSSC), 2004. NEHRP recommended provisions for seismic regulations for new buildings and other structures, 2003 edition (FEMA 450), Building Seismic Safety Council, National Institute of Building Sciences, Washington, DC, USA.

Castellaro, S & Mulargia, F., 2009. Vs30 estimates using constrained H/V measurements, *Bull. seism. Soc. Am.,* **99,** 761–773.

Çelebi, M., 1987. Topographical and geological amplifications determined from strong-motion and aftershock records of the 3 March 1985 Chile earthquake, *Bull. seism. Soc. Am.,* **77,** 1147–1167.

CEN, 2003. Eurocode (EC) 8: Design of structures for earthquake resistance – Part 1 General rules, seismic actions and rules for buildings, *EN, 1998–2001*, Brussels, Belgium.

Chatelain, J.L., Guillier, B., Cara, F., Duval, A.M., Atakan, K. & Bard, P.Y., SESAME WP02 team, 2008. Evaluation of the influence of experimental conditions on H/V results from ambient noise recordings, *Bull. Earthq. Eng.,* **6,** 33–74.

Chávez-García, F.J., Stephenson, W.R. & Rodríguez, M., 1999. Lateral propagation effects observed at Parkway, New Zealand: a case history to compare 1D vs 2D effects, *Bull. seism. Soc. Am.,* **89,** 718–732.

Cruz, E., Riddell, R. & Midorikawa, S., 1993. A study of site amplification effects on ground motions in Santiago, Chile, *Tectonophysics,* **218,** 273–280.

Fäh, D., Kind, F. & Giardini, D., 2001. A theoretical investigation of average H/V ratios, *Geophys. J. Int.,* **145,** 535–549.

Fäh, D., Kind, F. & Giardini, D., 2003. Inversion of local S-wave velocity structures from average H/V ratios, and their use for the estimation of site-effects, *J. Seism.,* **7,** 449–467.

Fäh, D. *et al*., 2006. The earthquake of 250 A.D. In Augusta Raurica, A real event with 3D site effect?, *J. Seismol.* **10,** 459–477.

Field, E.H. & Jacob, K.H., 1995. A comparison and test of various site-response estimation techniques, including three that are not reference-site dependent, *Bull. seism. Soc. Am.,* **85,** 1127–1143.

GeoE-Tech, 2007. Estudios sismicos en cuenca de Santiago perfiles de refracción sismica, Informe No. 2, www.geoe-tech.cl.

Goovaerts, P., 2000. Geostatical approaches for incorporating elevation into the spatial interpolation of rainfall, *J. Hydrol.,* **228,** 113–129.

Harkrider, D.G., 1964. Surface waves in multilayered elastic media, part 1, *Bull. seism. Soc. Am.* **54,** 627–679.

Holzer, T.L., Padovani, A.C., Bennett, M.J., Noce T.E. & Tinsely, J.C., 2005. Mapping v_s^{30} site classes, *Earthq. Spectra,* **21,** 353–370.

Horike, M., Zhao, B. & Kawase, H., 2001. Comparison of site response characteristics inferred from microtremor and earthquake shear waves, *Bull. seism. Soc. Am.,* **91**(6), 1526–1536.

International Conference on Building Officials, 1997. Uniform Building Code, in *International Conference on Building Officials,* Whittier, CA, USA, pp. 1411.

Isaaks, E.H. & Srivastava, R.M., 1989. Applied Geostatics, pp. 561, Oxford University Press, New York, NY, USA.

Iriarte, S., 2003. Impact of urban recharge on long-term management of Santiago Norte aquifer, Santiago, Chile, *Master thesis*. Waterloo University, Ontario, Canada.

Iriarte, S., Atenas, M., Aguirre & Tore, C., 2006. Aquifer recharge and contamination determination using environmental isotopes: Santiago basin, Chile: a study case, *Estudios de hidrología isotópica en América latina, International Atomic Energy Agency,* Section Isotope geology, Vienna, pp. 97–112.

Kitsunezaki, C. *et al.*, 1990. Estimation of P- and S-wave velocities in deep soil deposits for evaluating ground vibrations in earthquake, *J. JSNDS* **9,** 1–17.

Konno, K. & Ohmachi, T., 1998. Ground-motion characteristics estimated from spectral ratio between horizontal and vertical components, *Bull. seism. Soc. Am.,* **88**(1), 228–241.

Krige, D.G., 1951. A statistical approach to some mine valuations and allied problems at the Witwatersrand, *Master thesis*. University of Witwatersrand, Johannesburg, South Africa.

Lagos, J., 2003. Ignimbrita Pudahuel: caracterización geológica geotécnica orientada a su respuesta sísmica, *Master thesis*. Universidad de Chile, Santiago, Chile.

Laslett, G.M., 1994. Kriging and splines: An empirical comparison of their predicative performance in some applications, *J. Am. Stat. Assoc.,* **89,** 391–409.

Lermo, J. & Chavez-Garcia, F.J., 1994. Are microtremors useful in site response evaluation?. *Bull. Seism. Soc. Am.* **84**(5), 1350–1364.

Midorikawa, S., Riddell, R. & Cruz, E., 1991. Strong-ground accelerograph array in Santiago, Chile, and preliminary evaluation of site effects, *Earthq. Eng. Struct. Dyn.,* **20,** 403–407.

Nakamura, Y., 1989. A method for dynamic characteristics estimation of subsurface using microtremor on the ground surface, *Q. Rep. Railway Tech. Res. Inst.* **30,** 25–33.

Ortigosa, P. & Lástrico, R., 1971. Efecto sísmico. En informe de mecánica de suelos, *Informe No. 1,* Metropolitano de Santiago, Sec. Mec. Suelos, IDIEM, Universidad de Chile, Santiago, Chile, pp. 41–47.

Ohrnberger, M., Scherbaum, F., Krüger, F., Pelzing, R. & Reamer, S.K., 2004. How good are shear wave velocity models obtained from inversion of ambient vibrations in the Lower Rhine Embayment (N.W. Germany)?, *Bollettino di Geofisica teorica ed applicata* **45,** 215–232.

Paolucci, R., 2002. Amplification of earthquake ground motion by steep topographic irregularities, *Earthq. Eng. Struc. Dyn.* **31,** 1831–1853.

Park, S. & Elrick, S., 1998. Predictions of shear-wave velocities in southern California using surface geology, *Bull. seism. Soc. Am.* **88,** 677–685.

Parolai, S., Richwalski, S., Milkereit, C. & Fäh, D., 2006. S-wave velocity profiles for earthquake engineering purposes for the Cologne area (Germany), *Bull. Earthq. Eng.* **4,** 65–94.

Pasten, C.R., 2007. Respuesta sismica de la cuenca de Santiago, *PhD thesis*. Universidad de Chile, Santiago, Chile.

Picozzi, M., Parolai, S. & Albarello, D., 2005. Statistical analysis of noise horizontal-to-vertical spectral ratios (HVSR), *Bull. seism. Soc. Am.,* **95**(5), 1779–1786.

Pilz, M., Parolai, S., Leyton, F., Campos, J. & Zschau, J., 2009. A comparison of site response techniques using earthquake data and ambient seismic noise analysis in the large urban area of Santiago de Chile, *Geophys. J. Int.,* **178,** 713–728.

Sánchez-Sesma, F.J. & Luzon, F., 1995. Seismic response of three-dimensional alluvial valleys for incident P, S, and Rayleigh waves, *Bull. seism. Soc. Am.,* **85,** 269–284.

Scherbaum, F., Hinzen, K.G. & Ohrnberger, M., 2003. Determination of shallow shear wave velocity profiles in the Cologne Germany area using ambient vibrations, *Geophys. J. Int.,* **152,** 597–612.

Semblat, J.F., Duval, A.M. & Dangla, P., 2002. Seismic site effects in a deep alluvial basin: numerical analysis by the boundary element method, *Comput. Geotech.,* **29**(7), 573–585.

Strollo, A., Parolai, S., Jäckel, K.H., Marzorati, S. & Bindi, D., 2008a. Suitability of short-period sensors for retrieving reliable H/V peaks for frequencies less than 1 Hz, *Bull. seism. Soc. Am.* **98**(2), 671–681.

Strollo, A., Bindi, D., Parolai, S. & Jäckel, K.H., 2008b. On the suitability of 1 s geophone for ambient noise measurements in the 0.1–20 Hz frequency range: experimental outcomes, *Bull. Earthq. Eng.* **6**(1), 141–147.

Tokimatsu, K. & Miyadera, Y., 1992. Characteristics of Rayleigh waves in microtremors and their relation to underground structures, *J. Struct. Constr. Eng.,* **439,** 81–87.

Toshinawa, T., Matsuoka, M. & Yamazaki, Y., 1996. Ground-motion characteristics in Santiago, Chile, obtained by microtremor observations, in: *Proceedings of the 11th World Conference on Earthquake Engineering,* Paris, Paper 1764.

Valenzuela, G.B., 1978. Suelo de fundación del Gran Santiago, Inst. Invest. Geol. Santiago, Chile, Bol. 33

Wackernagel, H., 1998. Multivariate Statistics. An Introduction with Applications, pp. 257 , Springer, New York, USA.

Wald, D.J. & Allen, T.I., 2007. Topographic slope as a proxy for seismic site conditions and amplification, *Bull. seism. Soc. Am.,* **97,** 1379–1395.

Wills, C.J., Petersen, M.D., Bryant, W.A., Reichle, M.S., Saucedo, G.J., Tan, S.S., Taylor, G.C. & Treiman, J.A., 2000. A site-conditions map for California based on geology and shear wave velocity, *Bull. seism. Soc. Am.,* **90,** 187–208.

Wooleroy, E.W. & Street, R., 2002. 3D near-surface soil response from H/V ambient-noise ratios, *Soil Dyn. Earthq. Eng,.* **22,** 865–876.

Yamanaka, H. & Ishida, H., 1996. Application of generic algorithms to an inversion of surface-wave dispersion data, *Bull. seism. Soc. Am.,* **86,** 436–444.